Replica Correlation-Based Synchronization with Low Complexity and Frequency Offset Immunity

Kapseok Chang, Seung Chan Bang, and Hoon Kim

This paper investigates the multifarious nature of the long-term evolution (LTE) scheme and that of the modified LTE scheme for symbol timing synchronization (STS). This investigation allows us to propose a new replica correlation-based STS scheme to overcome the inherent weaknesses of the other two schemes. The proposed STS signal combines a gold sequence and a half sine wave in the time domain, whereas conventional STS signals specify either binary sequences or complex sequences in the time domain or in the frequency domain. In the proposed scheme, a sufficient correlation property is realized by the gold sequence, and robustness against the frequency offset (FO) is achieved through the sine wave. Compared to the existing LTE-related schemes, the proposed scheme can better achieve immunity to FO and reduction in detector complexity, as well as a low peak-to-average power ratio and a low detection error rate. Performance evaluations through analysis and simulation are provided in the paper to demonstrate these attributes.

Keywords: Frequency offset, PAPR, OFDM, complexity, symbol timing synchronization.

I. Introduction

Due to high spectral efficiency and robustness against multipath fading, orthogonal frequency division multiplexing (OFDM) has been widely adopted as the modulation technology in wireless communication standards. These standards include IEEE802.16m [1] and IEEE802.11n [2], as well as the 3rd Generation Partnership Project (3GPP) long-term evolution (LTE) [3], to which the chunk-based resource allocations [4], [5] are effectively applied. The LTE standard has been in the limelight as one of the 4th generation mobile communications. Just like in any other digital communication system, the specification of the synchronization signals is one of the pivotal standardization issues in OFDM systems. Any mobile station (MS) intending to access such OFDM systems must acquire symbol timing synchronization (STS) in the absence of knowledge about the initial carrier frequency offset (FO) and STS in the received signal [1]-[3], [6]-[9]. A poorer STS performance resulting from a higher initial FO leads to a longer latency in initial system access [6]-[9]. Generally, two types of detectors for STS are employed: aperiodic replica correlation (RC) [1], [3], [6], [9] and periodic differential correlation (DC) [2], [10]. Unlike IEEE802.11n, LTE has adopted RC because it provides a lower detection error rate (DER) (that is, higher STS accuracy) than DC, especially when there is a negligible FO. However, for a high FO, RC may suffer a higher detector complexity and experience higher DER performance when compared to DC, which leads to excessive battery drain at the MS [7]-[9]. On the other hand, since the peak-to-average power ratio (PAPR) may have a deleterious effect on the battery lifetime of the transmitter side in low-cost mobile applications due to nonlinear amplification, especially in OFDM, the drawback of high PAPR may outweigh all the

Manuscript received Nov. 7, 2012; revised May 10, 2013; accepted June 19, 2013.

This research was supported by the ICT Standardization program of MISP (The Ministry of Science, ICT & Future Planning).

Kapseok Chang (phone: +82 42 860 1639, kschang@etri.re.kr) and Seung Chan Bang (scbang@etri.re.kr) are with the Communications & Internet Research Laboratory, ETRI, Daejeon, Rep. of Korea.

Hoon Kim (corresponding author, hoon@incheon.ac.kr) is with the Department of Electronics Engineering, Incheon National University, Incheon, Rep. of Korea.

http://dx.doi.org/10.4218/etrij.13.0112.0764

potential benefits of OFDM-based systems [11].

Contribution and relation to previous work. Progressive studies related to the LTE-compliant STS signal were conducted in [12]-[14], which means that they focused on proposing the effective detecting schemes to acquire the STS at an MS. In [12], an optimized RC-based detection scheme for computing frequency-domain (FD) Zadoff-Chu (ZC) sequence elements was proposed. In [13], a robust time and frequency synchronization detection scheme based on a hybrid of DC and RC was proposed to realize both low detector complexity and high accuracy. In [14], the STS detection scheme based on RC and central self-correlation using the central-symmetric property (CSP) in ZC sequences was studied to reduce the detector complexity. The authors in [6] specified a modified LTE (MLTE) STS signal that lowers the DER under a high FO in an RC-based scheme. However, they made no reduction of computational detector complexity over LTE. On the other hand, there was no attention to the PAPR reduction in [6] and [12]-[14]. To resolve the shortcomings in [6], to reduce the inherent PAPR, and to offer immunity against the FO, this paper concentrates on proposing an STS signal that aligns with the work presented in [12] through [14] for the pursuit of further complexity reduction and accuracy through effective detection. Specifically, we propose a time-domain (TD) STS signal that is the product of a gold sequence and a half sine wave with an RC-based detector[1]. In this paper, we will compare our proposed scheme with LTE [3] and MLTE [6] through PAPR analysis, performance metrics (that is, complexity reduction, robustness against the FO, and correlation property), and DER evaluation.

The remainder of this paper is organized as follows. In section II, we provide a description of the system and signal models adopted in this work. In section III, the STS signals used in the existing and proposed schemes are described and their PAPRs are analyzed. A detailed description of the output of the detector and an analysis of the performance metrics are provided in section IV. The DER performances are provided in section V. Finally, conclusions are drawn in section VI.

Notation. $\mathbf{M}^{-1}$, $\mathbf{M}^{T}$, and $\mathbf{M}^{H}$ are the inverse, transpose, and complex conjugate transpose of matrix $\mathbf{M}$, respectively. Expression $\Xi_{a,b}\{\cdot\}$ denotes the expectation with the random variables a and b within the brackets. A circularly symmetric complex Gaussian random variable is $Z=X+jY\sim\mathcal{CN}(0, \sigma^2)$, where X and Y are independent and identically distributed. The (m, n)-th element of $\mathbf{M}$ is denoted by $(\mathbf{M})_{m,n}$. The m-th element of vector $\mathbf{v}$ is denoted by $(\mathbf{v})_m$. The $n\times1$ zero vector is denoted by $\mathbf{0}_n$. Lastly, the largest integral smaller than x is denoted by $\lfloor x \rfloor$.

1) While existing standards [1]-[3], [9], [15], [16] adopted solely either binary or complex sequences as STS signals in the TD or in the FD, we employ a non-flat signal with CSP to realize the FO immunity, as well as a binary gold sequence to achieve the sufficient correlation property.

II. System Signal Models

Figure 1 shows the frame structure of the LTE system, in which the time duration of a radio frame is 10 ms [3]. A frame consists of 10 subframes and each subframe is further organized into two time slots. The 20 time slots in each frame are indexed from 0 to 19, and the primary synchronization (identical to the STS named in this paper) and secondary synchronization (SS) signals are deployed at the last and second last OFDM symbols, respectively, in slots 0 and 10. The STS signals can be those of either the proposed scheme or all reference schemes [3], [6] described in this paper. As shown in this figure, the LTE frame structure contains two pairs of synchronization symbols spaced 5 ms apart. The STS signals assigned to slots 0 and 10 are identical so that the accumulation between these two STS signals can be performed for further STS performance improvement. On the other hand, the SS signals in these slots are different for cell identification.[2] Regardless of the system bandwidth adopted (between 1.25 MHz and 20 MHz), these synchronization signals occupy the 1.25-MHz center frequency band and spread over 64 subcarriers (the first and direct current subcarriers are null carriers) [3], [8]. Other subcarriers are used for control signaling and data transmission.

Let $s(k)$ be the FD STS signal, as shown in Fig. 1, with k being the subcarrier index. Ignoring the cyclic prefix (CP) duration of Nc samples, the $N\times1$ transmitted TD signal vector $\mathbf{x}$

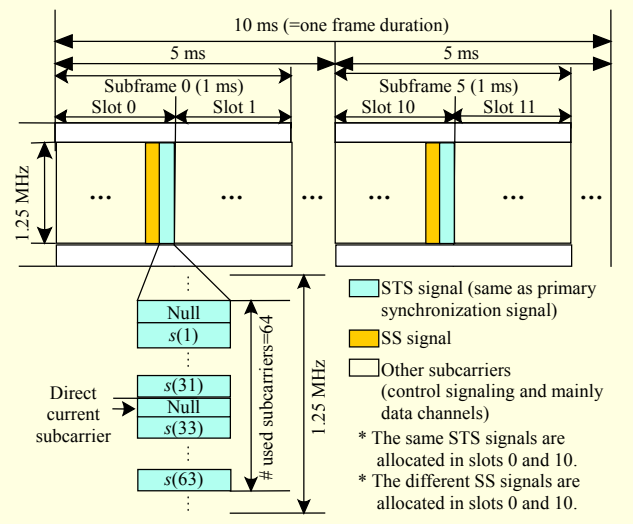

Fig. 1. Frame structure of LTE system.

2) The detailed description of cell identification is omitted so as to concentrate on the STS.

corresponding to the FD STS signal with N sample times (that is, $0 \le n < N$) is expressed as

$$\begin{aligned}\mathbf{x} &= [x(0) \ldots x(n) \ldots x(N-1)]^T \\ &= \mathbf{F}_N \mathbf{s} = \mathbf{F}_N [s(0) \ldots s(k) \ldots s(N-1)]^T,\end{aligned} \tag{1}$$

where $\Xi_x\{x(n)x^*(m)\} = E_s\delta(n-m)$ with the average transmitted power E_s and the Kronecker delta $\delta(\cdot)$ and where $\Xi_x\{x(n)\} = 0$. In (1), the $N \times N$ inverse discrete Fourier transform (IDFT) matrix $\mathbf{F}_N$ is given by

$$(\mathbf{F}_N)_{n,k} = \frac{1}{\sqrt{N}} e^{j\frac{2\pi nk}{N}}, \quad 0 \le n,k < N, \tag{2}$$

where N is the IDFT size corresponding to the system bandwidth [3], [8] (for example, N=1,024 for 10 MHz). In addition, the vector $\mathbf{s}$ in (1) is the $N \times 1$ FD STS signal vector, and it can be obtained from $\mathbf{x}$ in (1) and $\mathbf{F}_N$ in (2) as

$$\mathbf{s} = \mathbf{F}_N^{-1}\mathbf{x}. \tag{3}$$

The $(N+Nc) \times 1$ received baseband signal vector $\mathbf{r}$ corresponding to $\mathbf{x}$ in (1) at the beginning of the CP located just before the exact STS symbol timing can be represented as

$$\begin{aligned}\mathbf{r} &= \mathbf{E}\tilde{\mathbf{y}} + \mathbf{z} \\ &= \mathbf{E}\left[y([-Nc]_N) \cdots y([-1]_N)\ \mathbf{y}^T \right]^T + \mathbf{z} \\ &= \mathbf{E}[y([-Nc]_N) \cdots y([-1]_N)\ y(0) \cdots y(n) \cdots y(N-1)]^T \\ &\quad + [z(-Nc) \cdots z(n) \cdots z(N-1)]^T,\end{aligned} \tag{4}$$

where $[q]_N$ returns the modulo-N value of the integer q, with $[q]_N = N+q$ for $q<0$ and $[q]_N = q$ for $q \ge 0$. Also, $\mathbf{z}$ is the $(N+Nc) \times 1$ additive white Gaussian noise (AWGN) vector whose elements are complex Gaussian $\mathcal{CN}(0, N_0)$ random variables with zero mean and N_0 variance. Moreover, in (4), $\mathbf{E}$ is the $(N+Nc) \times (N+Nc)$ FO-related diagonal matrix, given by

$$\begin{aligned}\mathbf{E} &= \mathrm{diag}\{E(-Nc) \cdots E(-1)\ E(0) \cdots E(n) \cdots E(N-1)\} \\ &= \mathrm{diag}\{E(-Nc) \cdots E(-1)\ \hat{\mathbf{E}}\},\end{aligned} \tag{5}$$

where $\hat{\mathbf{E}}$ is the $N \times N$ diagonal matrix and $E(n) = \exp\{j2\pi\varepsilon n/N\}$ with ε representing the actual carrier FO between the transmitter and the receiver that is normalized to a subcarrier spacing of the effective OFDM symbol. Furthermore, assuming a frequency selective fading channel with multiple time-invariant paths at an MS, $\mathbf{y}$ in (4) before being influenced by the carrier FO mismatch between the transmitter and the receiver is expressed as follows, from (1), (2), [6]-[8], and [17]:

$$\mathbf{y} = \mathbf{F}_N \mathbf{H} \mathbf{s}, \tag{6}$$

where $\mathbf{H}$ is the $N \times N$ channel-related diagonal matrix and given by

$$\mathbf{H} = \mathrm{diag}\{H(0) \cdots H(k) \cdots H(N-1)\}. \tag{7}$$

In (7), $H(k)$ is expressed as [8], [17]

$$H(k) = \sum_{l=0}^{L-1} \alpha(l) e^{-j\frac{2\pi k \tau_l}{N}}, \tag{8}$$

with L, $\alpha(l)$, and τ_l representing the maximum multipath, the discrete-time impulse response where $\sum(\Xi_\alpha\{|\alpha(l)|^2\}) = 1$, and the path delay of the l-th path component expressed in terms of the sampling time, respectively.

III. STS Signal Description and Analysis

1. Reference STS Signals

The reference STS signals used for performance comparison are those of the LTE [3] and the MLTE [6]. In the LTE scheme, the FD STS signal $s(k)$ as shown in (1) and Fig. 1 is given by

$$s(k) = \sqrt{E_s} e^{-j\frac{\pi u(k-1)k}{N-1}}, \quad 1 \le k < N, \tag{9}$$

where N=64, $s(0)=s(32)=0$, and u is the length-(N–1) sequence root index. Of the N–2 possible ZC sequence indices, it is elucidated that the three sequences associated with the indices 25, 29, and 34 provide the best performances for STS. For comparison, u=25 is selected in this paper since the STS performances for these three indices are almost identical [8], [18]. As for the MLTE scheme, the FD STS signal is based on a distribution of a base sequence and its minus as follows, at odd k,

$$s(k) = \begin{cases} \sqrt{E_s} e^{\frac{-j\pi v\left\lfloor \frac{k-1}{2} \right\rfloor \left(\left\lfloor \frac{k-1}{2} \right\rfloor + 1 \right)}{\frac{N}{2}-1}} = \hat{s}(k) & \text{for } 1 \le k < \frac{N}{2}, \\ -\hat{s}(k) & \text{for } \frac{N}{2}+1 \le k < N, \end{cases} \tag{10}$$

where N=64, $s(0)=s(32)=0$ that are the same as those in the LTE scheme, and v is the length-(N/2–1) ZC sequence root index with v=1 [6]. At even k, $s(k) = -\hat{s}(k)$ for $1 \le k < N/2$ and $s(k) = \hat{s}(k)$ for $N/2+1 \le k < N$.

2. Proposed STS Signal

We propose an STS signal based on a TD multiplication of a half sine wave by a gold sequence $W(n)$, The half sine wave (that is, the normalized frequency of the sine wave is set to 1/2) and gold sequence are introduced to realize FO immunity and a desirable correlation property during synchronization, respectively. In our indication, in the time domain, rather than the STS signals having flat amplitude patterns, the non-flat convex (for example, half sine wave) or concave signals should realize the FO immunity. Concretely, to clearly observe the immunity, it is assumed that the normalized carrier FO ε is set to be 1. This assumption implies that the received signal

multiplied with the conjugated STS signal at the receiver side (see (4) and (14)) is multiplied by each of the full cosine (real component) and cosine (imaginary component) waves caused by the carrier FO, as shown in Fig. 2. If the ideally multiplied received signal from the starting point of zero STO is flat, as in Fig. 2, the resultant value of (14) is zero (real component: summation after the multiplication of "1" by "cos(2π(n–1)/64)"; imaginary component: summation after the multiplication of "1" by "sin(2π(n–1)/64)") in the case of no fading and no noise being zero, which leads to the weakness against the FO. In contrast, if the ideally multiplied received signal has the pattern of the half sine wave, the resultant value is not zero (real component: non-zero; imaginary component: zero), as shown in Fig. 2, which leads to the significant degree of power against the FO. We will return to this FO immunity topic regarding the current LTE STS signal in part B of subsection IV.2.

In addition, as generally known, the autocorrelation property of the half sine wave form itself is much worse than those of other orthogonal or quasi-orthogonal sequences, such as the Hadamard code, the m-sequence, and the ZC sequence. So as to overcome the weakness of the autocorrelation property, we apply $W(n)$ to the half sine wave.

In the following, we will refer to this scheme that combines the half sine wave with $W(n)$ as the GSW scheme. The GSW signal $x(n)$ in (1) is expressed as

$$x(n)=\sqrt{\frac{2E_s(N-2)}{N}}W(n)\sin\left(\frac{n\pi}{N}\right),\ 0\le n<N, \qquad (11)$$

where N is set to 64 as in subsection III.1. In (11), $W(n)$ is defined as

$$W(n)=\begin{cases} G_1(n-1)\oplus G_2([n-1+w]_N) & \text{for } 1\le n<\frac{N}{2}, \\ W(n)=W\left(n+1-\frac{N}{2}\right) & \text{for } \frac{N}{2}\le n<N-1, \end{cases} \qquad (12)$$

where $W(0)=W(N-1)=1$, $\oplus$ denotes the exclusive-OR operation, and w is the GSW sequence index (w=5), chosen based on the preliminary evaluation results obtained by using the correlation-property performance metric 3, which will be shown in part C of subsection IV.2. In addition, $G_1(n-1)$ and $G_2([n-1+w]_N)$ in (12) are binary pseudo-noise sequences [19] corresponding to the generator polynomials x^5+1 and x^5+x^4+x+1, respectively.[3] Moreover, the factor $2(N-2)/N$ in (11) is applied to maintain the same average power maintained in the reference schemes. We note that through the operation in (3), the GSW signal can be converted and embedded into the LTE-like frame in the FD.

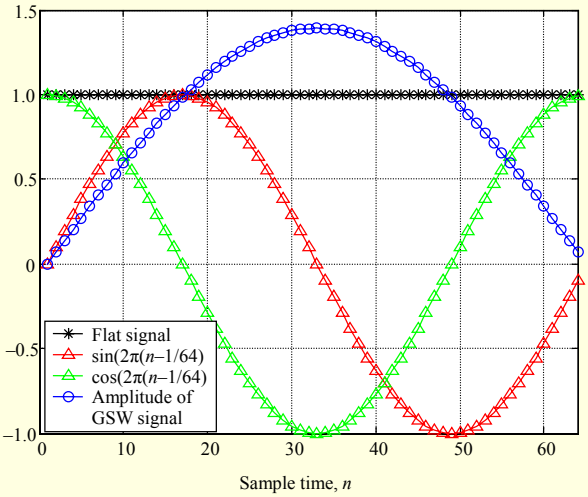

Fig. 2. STS signal patterns.

3. PAPR Analysis

A main disadvantage of OFDM on the transmitter side is the high PAPR of the transmitted signal that includes a synchronization signal. In the worst example, when the signals are added constructively, the peak power may be the multiplication of the total number of subcarriers by the average power. The power consumption of a power amplifier is swayed much more so by the peak power than the average power. Since the spectral growth of the OFDM signal in the form of intermodulation among subcarriers and out-of-band radiation due to high peaks should be prevented, the power amplifier shall be operated in its linear region, which leads to the aggravation of the power efficiency. These may have a detrimental effect on battery lifetime [11], [20]. For this reason, as part of simply appraising a comparative advantage, we compare the PAPRs of the GSW, LTE, and MLTE schemes, as shown in Table 1, where the PAPR is defined as

$$\text{PAPR}=\frac{\max\limits_{0\le n<N}|x(n)|^2}{\frac{1}{N}\sum\limits_{n=0}^{N-1}|x(n)|^2}. \qquad (13)$$

Table 1 shows that the PAPR of the proposed GSW scheme is lower than that of LTE by 0.8 dB and that of MLTE by 2.3 dB[4].

3) This well-known binary gold sequence is employed as an example in this paper for the proposed STS signal design. On that account, any binary sequence may be applied if it demonstrates a sufficient correlation property. In addition, how come we prefer to binary sequences to complex ones is because of reducing the detector complexity as exposed in Table 2.

4) It is noted that the LTE, MLTE, and GSW signals for STS may sufficiently display lower PAPR properties than the data signal in LTE-like systems. However, when the transmission power of an STS signal is higher than that of a data signal for the robust initial system-access setup as well as the peak power of the STS signal is between the linear and nonlinear regions of a transmission amplifier, the PAPR advantage of the GSW signal is able to be meaningful.

Table 1. PAPR value for each STS scheme.

STS scheme	LTE	MLTE	GSW
PAPR (dB)	3.8	5.3	3.0

Thus, the GSW scheme fulfills the lowest PAPR among them.

IV. Detector Description and Analysis

1. Detector Description

The detector of STS requires an MS to perform a noncoherent detection[5] that finds the starting sample time of the synchronization signal (that is, sample timing offset [STO], θ). The noncoherent detection can be optimally performed by maximizing a decision variable (DV) over all possible hypothesis STOs, where the DV is actually a cross-correlation between the transmitted STS signal and the received signal [8]. For the optimality of the detection, we assume perfect automatic gain control (AGC) in this paper on the basis that the optimal maximum likelihood of time synchronization is the same as the maximization of the cross-correlation under the AGC employed in practice [7], [13], [21]. The starting sample time of the STS signal can be identified by the MS as

$$\left\{\hat{\theta}\right\} = \arg\max_{\theta}\left\{D_{\theta}\left(\varepsilon,\alpha(l),\mathbf{z}\right)\right\} = \operatorname*{argmax}_{\theta}\left\{\frac{\left|\mathbf{x}^{H}\mathbf{r}_{\theta}\right|^{2}}{E_{s}}\right\},\ 0\le\theta\le Nc, \tag{14}$$

where $D_{\theta}(\varepsilon, \alpha(l), \mathbf{z})$ is the DV for STS that is a function of the FO ε in (5), the multipath profile $\alpha(l)$ in (8), and the noise vector $\mathbf{z}$ in (4). Also, $\mathbf{x}^{H}$ in (14) is the local replica for cross-correlation, which is identical to the complex conjugate transpose of vector $\mathbf{x}$ in (1). Moreover, $\mathbf{r}_{\theta}$ in (14) is the $N\times1$ vector comprising the elements starting from sample ($Nc-\theta$) to sample ($N-1+Nc-\theta$) extracted from the vector $\mathbf{r}$ in (4).

2. Performance Metrics and Analysis

In addition to higher PAPR, fundamentally, the higher the complexity of the detector employed in a certain STS scheme is, the more the battery lifetime is shortened. It is also much more likely that the frequent sample timing misdetection (strongly related with the detector's weaknesses against the FO) leads to a longer latency in the initial system access and results in excessive battery draining at the MS [7]-[9]. Thus, it is greatly informative in this subsection to analyze these factors with the three performance metrics presented below.

Table 2. Detector complexity of each STS scheme at every STO in terms of number of real-value multiplications.

STS scheme	LTE	MLTE	GSW
Complexity	$4N$	$4N$	$2N$

A. Metric 1: Complexity Reduction

Let us analyze the detector complexity required to generate the DV $\mathbf{x}^{H}\mathbf{r}_{\theta}$ in (14) for each STS scheme at every STO in terms of the number of real-value multiplications, which is the main computational burden [17], [22], [23]. Since the FD ZC-based signals of the LTE and MLTE schemes as specified in (9) and (10), respectively, are complex, their signals are easily identified to be complex in the time domain. This brings us to the salient point about the GSW signal in (11): the time-domain version of this signal is real.

As shown in Table 2, while both the LTE scheme and the MLTE scheme require $4N$ real multiplications to compute the DV in (14), the proposed GSW scheme needs $2N$. As such, the computational complexity of the GSW scheme is only half that of each of the other schemes.[6]

B. Metric 2: Robustness against FO in Simple FO Condition

In general, if there is no FO, then the DV in (14), as a function of STO, will peak when the offset is zero (that is, θ=0). However, in the presence of the FO, the DV may have comparable values at other STOs, which will result in a sample-level timing error and a higher DER performance. Accordingly, we herein analyze the robustness against the FO of the proposed GSW signal and of the reference STS signals.

Firstly, consider the following simple FO conditions: no fading, that is, L=1 and $\alpha(0)$=1 in (8); high FO, that is, ε=1 in (5); no noise, that is, $z(n)$=0 in (4); and normalized transmit power, that is, E_s=1 in (1). Setting ε to be 1 is initially introduced to schematically and mathematically observe the effect of the FO on the DV performance. The DV in (14) at a perfect STO (that is, θ=0) is redefined as follows, from (1), (5), and (6):

$$D_{0}(\varepsilon,1,\mathbf{0}_{N}) = \left|\mathbf{x}^{H}\mathbf{r}_{0}\right|^{2} = \left|\mathbf{x}^{H}\hat{\mathbf{E}}\mathbf{F}_{N}\mathbf{s}\right|^{2} = \left|\mathbf{x}^{H}\hat{\mathbf{E}}\mathbf{x}\right|^{2} = \left\{\sum_{n=0}^{N-1}D_{R}(n)\right\}^{2} + \left\{\sum_{n=0}^{N-1}D_{I}(n)\right\}^{2}, \tag{15}$$

5) The coherent detection requires the knowledge of channel attenuation, which is unavailable at the STS phase.

6) It is noted that the central symmetric property can be commonly applied to all of GSW, LTE, and MLTE schemes to further reduce their complexity by a factor of 1/2 in [14].

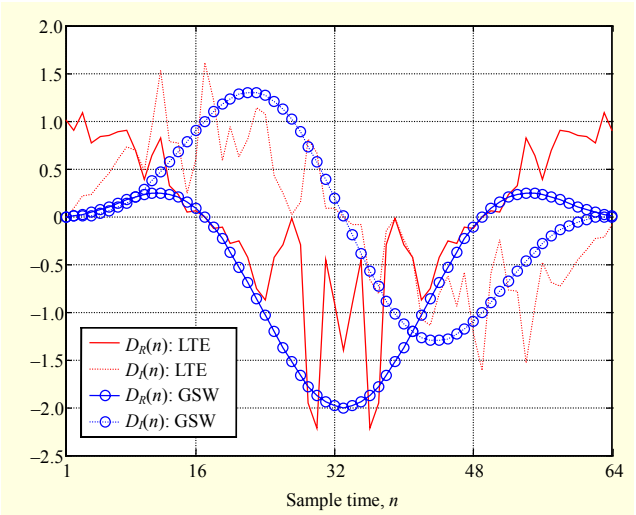

Fig. 3. Waveforms vs. sample time index n in terms of $D_R(n)$ and $D_I(n)$ in simple FO condition with ε=1 and without fading and noise.

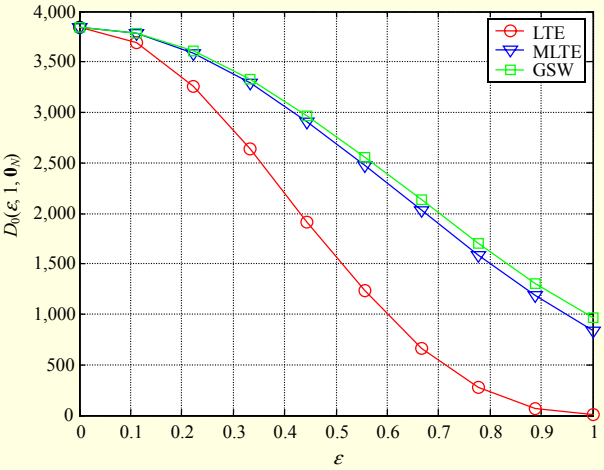

Fig. 4. $D_0(\varepsilon, 1, \mathbf{0}_N)$ vs. FO ε in simple FO condition without fading and noise.

with the definitions

$$D_R(n) \triangleq \text{Real}\left\{\left(\mathbf{x}^H\right)_n \left(\hat{\mathbf{E}}\mathbf{x}\right)_n\right\},$$
$$D_I(n) \triangleq \text{Imag}\left\{\left(\mathbf{x}^H\right)_n \left(\hat{\mathbf{E}}\mathbf{x}\right)_n\right\}, \quad (16)$$

where Real{g} and Imag{g} denote the real and imaginary components of g, respectively.

Figure 3 shows the waveforms of $D_R(n)$ and $D_I(n)$ for both the LTE scheme and the proposed GSW scheme as a function of sample time index n, where both $D_R(n)$ and $D_I(n)$ are obtained from (16). The curves labeled "GSW" are for the proposed scheme, while those labeled "LTE" are for the LTE scheme. For the LTE signals, the sum of all the imaginary components, that is, $\sum_n\{D_I(n)\}$, is almost zero. The same is true for the sum of all the real components, that is, $\sum_n\{D_R(n)\}$. This means the detector output, that is, $D_0(1, 1, \mathbf{0}_N)$ with ε=1 in (15), is zero for the LTE scheme for this particular channel condition. In contrast, for the proposed GSW scheme, while $\sum_n\{D_I(n)\}$ is zero, $\sum_n\{D_R(n)\}$ is not, which results from the non-flat property of the half sine waveform with CSP. Accordingly, the net result is that the detector output for GSW is larger than that for LTE, so the GSW scheme may offer a higher detection probability than the LTE scheme.

Secondly, so as to evaluate the robustness of each STS scheme according to the FO, we consider the following simple FO conditions: no fading, that is, L=1 and $\alpha(0)$=1 in (8); no noise, that is, $z(n)$=0 in (4); and normalized transmit power, that is, E_s=1 in (1). The DV from (14) under this condition, that is, $D_0(\varepsilon, 1, \mathbf{0}_N)$ in (15) at a perfect STO in the range of $0 \le \varepsilon \le 1$, is used for evaluation. Figure 4 shows the DV result of each STS scheme as a function of ε. From the results in Fig. 4, it can be seen that the GSW scheme outperforms the LTE scheme. Also, the GSW scheme attains a comparable performance to that of the MLTE scheme. However, this similarity may be muted if we take into account that the complexity and PAPR of the MLTE scheme are higher than those of the GSW scheme.

C. Metric 3: Correlation Property in Multipath Channel

Lastly, by using the DV in the range of $0 \le \theta \le 5$ in (14), let us examine the correlation property of each STS scheme under the typical urban channel with six paths (TU-6) [24], AWGN in (4), and E_s/N_0=0 dB. The cases of a zero FO (that is, ε=0) and a higher FO (that is, ε=2/3) [6], [8] are considered in this evaluation. Since the fading channel $\alpha(l)$ and the noise vector $\mathbf{z}$ are random variables, we obtain the average DV (that is, $\Xi_{\alpha\mathbf{z}}\{D_\theta(\varepsilon, \alpha(l), \mathbf{z})\}$, the average of $D_\theta(\varepsilon, \alpha(l), \mathbf{z})$ (14) over $\alpha(l)$ and $\mathbf{z}$) so as to statistically observe the DV performance for each of the STS schemes. Concretely, we employ the Monte Carlo simulation with 10,000 trials to get the average DV level for each of the STS schemes. Therefore, 10,000 instant DV levels are obtained for each combination of the STO and the STS scheme, and the sum of those values is divided by 10,000 to obtain the average DVs.

Figure 5 shows the average DV as a function of θ for each STS scheme, wherein a certain STS scheme exhibiting the property of the highest peak at a perfect STO (that is, θ=0) is beneficial even though a correct STS detection is declared if the detected STO is within half the CP duration [25]. From the results illustrated in Fig. 5, it can be concluded that in the case of the zero FO and the higher FO, all of the STS schemes exhibit this property, and every STS scheme provides an almost identical performance. On the other hand, in the case of the higher FO, the average DV of the LTE scheme is much worse than those of the MLTE and GSW schemes that are

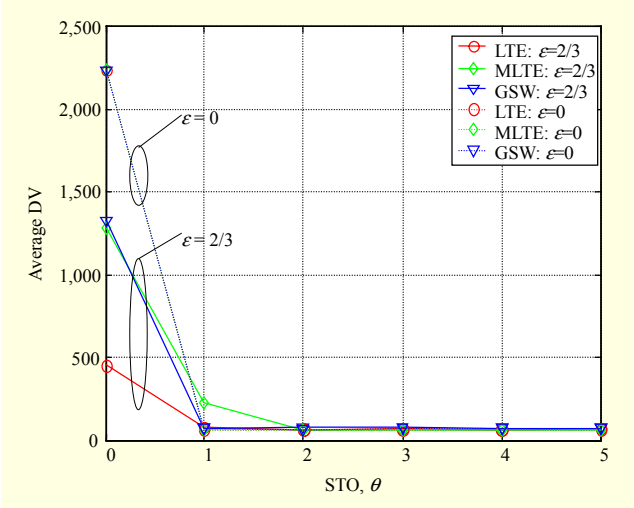

Fig. 5. $\Xi_{\alpha z}\{D_\theta(\varepsilon, \alpha(l), \mathbf{z})\}$ vs. STO θ with each of ε=0 and ε=2/3 in TU-6 channel at E_s/N_0=0 dB.

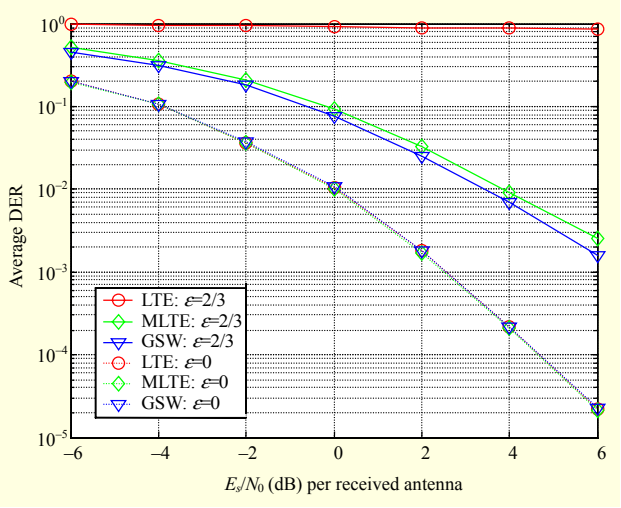

Fig. 6. DER vs. E_s/N_0 per received antenna with ε=0 and ε=2/3 in TU-6 channel with mobile velocity of 1 km/h.

comparable to one another, as in the performance metric 2 of part B of subsection IV.2. Interestingly, the GSW signal employs the non-flat sine wave, which may lead to significant average DVs at imperfect STOs (that is, $\theta \neq 0$). Nevertheless, as shown in Fig. 5, the average DVs at these STOs in the GSW scheme are almost the same as those of the LTE and MLTE schemes, which implies that the sufficient correlation property of the binary gold sequence is exhibited in the GSW scheme.

V. DER Evaluation

The DER performance of each STS scheme is evaluated with the LTE physical layer specification [3] and the following detailed parameter settings: a system bandwidth of 1.25 MHz (that is, N=64), a common carrier frequency of 2 GHz, a single cell model, no transmit diversity, and two-branch equal-gain combining diversity. The channel model is the TU-6 [24] with mobile velocities of 1 km/h and 100 km/h. Also, any accumulation between adjacent STS signals (for example, contiguous STS signals within more than one frame are combined for synchronization) is not performed to evaluate the DER performance under the condition of the numerical study of subsection IV.2. Moreover, throughout the evaluation, the MS-specific data signals are always loaded so as to realize the real scenario. Furthermore, the transmitted power for the STS signals is the same as that of the data signals, and, lastly, in evaluating the DER of STS, a correct detection is declared if the detected timing $\hat{\theta}$ in (14) is within half the CP duration (Nc=5 corresponding to N=64).

Figures 6 and 7 show the DER performances of each STS scheme as a function of E_s/N_0 with the mobile velocities of 1 km/h and 100 km/h, respectively. It is elucidated that the

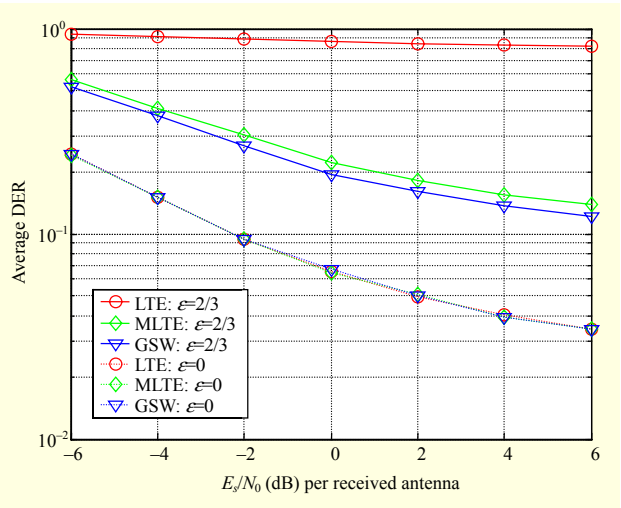

Fig. 7. DER vs. E_s/N_0 per received antenna with ε=0 and ε=2/3 in TU-6 channel with mobile velocity of 100 km/h.

results shown in Fig. 6 are consistent with the analyses presented in subsection IV.2 from the following observations: there is no DER difference at ε=0; at ε=2/3, the LTE scheme provides the worst DER performance and the GSW and MLTE schemes demonstrate comparable performances. In addition, it is revealed that there is no performance trend difference between the case of 1 km/h (Fig. 6) and that of 100 km/h (Fig. 7) in terms of DER. Moreover, it is observed that for both the MLTE scheme and the GSW scheme, a better DER performance results from a lower velocity.[7] If the drawbacks of the MLTE scheme are not overlooked, as mentioned at the end

7) This observation results from an absence of time diversity [7], [8], which means that if one of the accumulation techniques is employed, the observation may be reversed from the fact that the higher the mobile velocity, the larger the time diversity gain.

of part B of subsection IV.2, employing the proposed GSW scheme can be recommended.

VI. Conclusion

In this paper, we observed the weak points in the LTE and modified LTE schemes for STS. This observation enabled us to propose an STS scheme. In the proposed scheme, the proposed signal is the product of a binary sequence and a half sine wave. It was found through analysis and evaluation that the proposed scheme offers a lower PAPR, a lower detector complexity, and more robustness against the frequency offset than any other STS scheme. Since higher STS accuracy in conjunction with lower detector complexity and higher power efficiency is indispensable, the multifarious convincing aspects reported in this paper provide beneficial information on designing an STS signal.

References

[1] IEEE Std. 802.16m D12.0, *Part 16: Air Interface for Fixed and Mobile Broadband Wireless Access Systems-Advanced Air Interface*, IEEE Standard for Local and Metropolitan Area Networks, Feb. 2011.

[2] IEEE Std. 802.11n D4.0, *Part 11: Wireless LAN Medium Access Control (MAC) and Physical Layer (PHY) Specifications: Amendment 4: Enhancements for Higher Throughput*, IEEE Standard for Local Area Networks, March 2008.

[3] TS36.211 v10.0.0, *Physical Channels and Modulation (Release 10)*, 3GPP TSG RAN1, Dec. 2010, pp. 92-96.

[4] H. Zhu and J. Wang, "Chunk-based Resource Allocation in OFDMA Systems-Part I: Chunk Allocation," *IEEE Trans. Commun.*, vol. 57, no. 9, Sept. 2009, pp. 2734-2744.

[5] H. Zhu and J. Wang, "Chunk-Based Resource Allocation in OFDMA Systems-Part II: Joint Chunk, Power and Bit Allocation," *IEEE Trans. Commun.*, vol. 60, no. 2, Feb. 2012, pp. 499-509.

[6] K. Chang and Y. Han, "Robust Replica Correlation-based Symbol Synchronization in OFDM Systems," *Electron. Lett.*, vol. 44, no. 17, Aug. 2008, pp. 1024-1025.

[7] H. Meyr, M. Moeneclaey, and S.A. Fechtel, *Digital Communication Receivers: Synchronization, Channel Estimation, and Signal Processing*, New York: Wiley-Interscience, Oct. 2001.

[8] I.T.S. Sesia and M. Baker, *LTE — The UMTS Long Term Evolution: From Theory to Practice*, Chichester: John Wiley & Sons Ltd., 2009.

[9] H. Holma and A. Toskala, *WCDMA for UMTS*, Wiley, 2000.

[10] T.M. Schmidle and D.C. Cox, "Robust Frequency and Timing Synchronization for OFDM," *IEEE Trans. Commun.*, vol. 45, no. 12, Dec. 1997, pp. 1613-1621.

[11] S.H. Han and J.H. Lee, "An Overview of Peak-to-Average Power Ratio Reduction Techniques for Multicarrier Transmission," *IEEE Wireless Commun.*, 2005, pp. 56-65.

[12] M.M. Mansour, "Optimized Architecture for Computing Zadoff-Chu Sequences with Application to LTE," *IEEE GLOBECOM*, 2009.

[13] W. Xu and K. Manolakis, "Robust Synchronization for 3GPP LTE Systems," *IEEE GLOBECOM*, Miami, FL, USA, 2010.

[14] Z. Zhang, H. Kayama, and C. Tellambura, "New Joint Frame Synchronization and Carrier Frequency Offset Estimation Method for OFDM Systems," *Euro. Trans. Telecommun.*, vol. 20, no. 4, June 2009, pp. 413-430.

[15] 3GPP TS45.001, *Physical Layer on the Radio Path: General Description (Release 4)*, 3GPP TSG RAN, Oct, 2000.

[16] IEEE Std. 802.11ad D9.0, *Part 11: Wireless LAN Medium Access Control (MAC) and Physical Layer (PHY) Specifications: Amendment 3: Enhancements for Very High Throughput in the 60 GHz Band*, IEEE Standard for Local Area Networks, July 2012.

[17] K. Chang, K.Y. Kim, and D.H. Kim, "Reduction of Doppler Effects in OFDM Systems," *IEEE Trans. Consum. Electron.*, vol. 52, no. 4, Nov. 2006, pp. 1159-1166.

[18] LG, "P-SCH Design," *3GPP Tech. Doc.*, Tdoc R1-072860, 3GPP TSG RAN WG1 #49 bis, Orlando, FL, USA, June 2007.

[19] A.J. Viterbi, *CDMA: Principles of Spread Spectrum Communication*, Reading, MA: Prentice Hall, 1995.

[20] X. Ouyang et al., "Partial Shift Mapping for PAPR Reduction with Low Complexity in OFDM Systems," *ETRI J.*, vol. 34, no. 2, Apr. 2012, pp. 268-271.

[21] J.J. van de Beek, M. Sandell, and P.O. Börjesson, "ML Estimation of Time and Frequency Offset in OFDM Systems," *IEEE Trans. Signal Process.*, vol. 45, no. 7, July 1997, pp. 1800-1805.

[22] Q. Quan, "A Polynomial Complexity Optimal Multiuser Detection Algorithm Based on Monotonicity Properties," *ETRI J.*, vol. 32, no. 3, June 2010, pp. 479-481.

[23] X. Jiao and M.A. Armand, "On a Reduced-Complexity Inner Decoder for the Davey-MacKay Construction," *ETRI J.*, vol. 34, no. 4, Aug. 2012, pp. 637-640.

[24] 3GPP TR25.943 v8.0.0, *Technical Specification Group Radio Access Networks: Deployment Aspects*, Dec. 2008.

[25] M. Speth, F. Classen, and H. Meyr, "Frame Synchronization of OFDM Systems in Frequency Selective Fading Channels," *IEEE VTC*, vol. 3, May 1997.

Kapseok Chang received his M.S. (1999) and Ph.D. (2005) degrees from KAIST, Daejeon, Rep. of Korea. He has been with ETRI as a full-time senior researcher since July 2005. Additionally, since September 2009, he has been an affiliated professor at the University of Science and Technology, Daejeon, Rep. of Korea. From March 2011 to February 2013, he was with the School of Engineering Science, Simon Fraser University, Burnaby, BC, Canada as a visiting professor. During his Ph.D. study, he won the Brain Korea Scholarship. From ETRI in 2007 and IEEE 802.11ad in 2012, he received the Best Patent award and the Certificate of Appreciation, respectively. In November 2010, he was included in one of the Marquis Who's Who directories. In his main work, he made the standardization activities of 3GPP LTE (2005-2007) and IEEE 802.11ad (2009-2010) with these developments. His research has spanned smart antennas, MIMO, synchronization, network coding, full-duplex-based cooperative relay, and D2D communication.

Seung Chan Bang is currently working at ETRI, Daejeon, Rep. of Korea. He received his B.S., M.S., and Ph.D. degrees from the School of Electronics Engineering, Seoul National University (SNU), Seoul, Rep. of Korea, in 1984, 1986, and 1994, respectively. He joined ETRI in 1994. He was involved in developing the IS-95 CDMA system from 1994 to 1996. For IMT-2000, he was involved in developing the standard technologies of cdma2000 and the W-CDMA system from 1997 to 1999 and W-CDMA modem technology from 2000 to 2001. After IMT-2000, he participated in the national 4G project with respect to smart antennas and LTE, from 2002 to 2008. Now, he is in charge of ETRI's wireless transmission research department, in which 5G enabling technologies are being developed.

Hoon Kim received his B.S., M.S., and Ph.D. degrees in electrical engineering from the Korea Advanced Institute of Science and Technology (KAIST), Rep. of Korea in 1998, 1999, and 2004, respectively. He worked with the Samsung Advanced Institute of Technology (SAIT) from 2004 to 2005 and served as a senior engineer in the Communications and Networks Laboratory Division, joining the project of design and performance analysis of radio transmission technology for beyond 3G and 4G mobile communication systems. He worked with the Ministry of Information and Communications (MIC) from 2005 to 2007 and served as a deputy director in the Broadband Communications Division, promoting policies for the broadband communications industry, such as WiMAX and NGN. He was a visiting scholar at Stanford University during 2007 and 2008, developing radio resource management algorithms and cross layer optimization schemes for 4G mobile communications systems. He is currently with the Department of Electronics Engineering at Incheon National University as a member of the faculty. His research interests include performance evaluation of mobile communication systems, radio resource management schemes, and optimization of mobile systems operation. He is a member of KICS, IEEK, IEEE, and IEICE.